Available online at www.sciencedirect.com
SCIENCE DIRECT®
ELSEVIER
International Journal of Plasticity xxx (2005) xxx–xxx
INTERNATIONAL JOURNAL OF Plasticity
www.elsevier.com/locate/ijplas

Geometrical localization analysis of gradient-dependent parabolic Drucker–Prager elastoplasticity

S.M. Vrech, G. Etse *

Center for Numerical and Computational Methods in Engineering, University of Tucumán, Muñecas 730, 10A, 4000 Tucumán, Argentina

Received 20 March 2005

Abstract

In this work, the geometrical method for the analysis of the localization properties of the thermodynamically consistent gradient-dependent parabolic Drucker–Prager elastoplastic model is presented. From the analytical solution of the discontinuous bifurcation condition of small strain gradient-dependent elastoplasticity, the elliptical envelope for localization is formulated in the coordinates of Mohr. The tangency condition of the localization ellipse with the major principal circle of Mohr defines the type of failure (diffuse or localized) and the critical directions for discontinuous bifurcation.

The results of the geometrical localization analysis illustrate the capability of the gradient-dependent elastoplastic Drucker–Prager material to suppress the discontinuous bifurcations of the related local or classical elastoplastic model formulation that take place when the adopted hardening/softening modulus $\bar{H}$ equals the critical (maximum) one for localization $\bar{H}_c$. On the other hand, the results in this work also demonstrate that the thermodynamically consistent gradient-dependent Drucker–Prager model may lead to discontinuous bifurcation not only when the characteristic length l turns zero but also when $\bar{H} < \bar{H}_c$.

Keywords: Non-local constitutive model; Gradient elastoplasticity; Localized failure analysis

* Corresponding author. Tel: +54 381 4364093x7784; fax +54 381 4226151.
E-mail address: getse@herrera.unt.edu.ar (G. Etse).

0749-6419/$ - see front matter © 2005 Published by Elsevier Ltd.
doi:10.1016/j.ijplas.2005.07.002

1. Introduction

It has been widely accepted that when quasi-brittle or ductile materials are sufficiently deformed into the inelastic regime, they exhibit spatial discontinuities of the kinematic fields. The formation of cracks and shear bands observed in experiments in cementitious and granular materials, as well as in metals are typical examples of localized failure mechanisms.

There were several theoretical attempts to capture the onset of localization and to determine the direction and the amplitude of these cracks or shear bands. Following the original works by Nadai (1931), Thomas (1961), Hill (1962), Rudnicki and Rice (1975), recently many authors studied the problem in a systematic manner. Using the flow theory of plasticity, the theory of continuum damage and the viscoplastic theory, they developed mathematical conditions governing the failure behavior, see a.o. Sobh (1987), Perič (1990), Ottosen and Runesson (1991), Willam and Etse (1990), Sluys (1992), Rizzi et al. (1995), Etse and Willam (1999).

The solution at the boundary value or structural level requires the implementation of strain-softening material models in finite element codes. In this case, the problem of mesh dependence strongly affects the computational solution, when the governing equations turn ill-posed.

To solve the mesh sensitivity of the computational predictions of strain-softening material models, two possible strategies are at side. On one side, to improve the finite element technology by developing both standard finite element formulations, which are able to follow the post-bifurcation localization using realignment methods, and enhanced finite elements with discontinuous interpolation capabilities. On the other side, to regularize the description of the material behavior at the constitutive level. However, a combination of both approaches seems to be the most effective strategy.

In the regularization approach, the medium is considered to remain a continuum, with high deformation gradients being concentrated into a finite small region of the body. This leads to enriched material formulations that can be based on both local and non-local approaches. The most relevant example of the first one are the fracture energy-based constitutive formulations that lead to dissipation-objective regularization of the local constitutive theory, e.g. (Willam et al., 1984; Bažant, 1986). In the non-local approach, the gradients of the displacement function are evaluated in the vicinity of the material point, thus a spatial average is taken into account to evaluate the point value. This is accomplished by defining suitable weighted averages (non-local formulations) or gradients (gradient formulations) of a selection of thermodynamic variables.

Enhanced gradient material theories formulate constitutive relations on the continuum level that are used to solve the gap between the micro- and macromechanical description level, see Gao et al. (1999) and Abu Al-Rub Rashid and Voyiadjis (2004). In the literature, different frameworks of gradient-dependent plasticity theories may be recognized and they can be classified from different points of view. As pointed out by Huang et al. (2004), who presented a conventional theory of mechanism-based strain gradient plasticity that excludes higher-order stress, the classification may be based on the inclusion or not of this type of higher-order functions that requires extra

boundary conditions. Alternatively, gradient-dependent plasticity theories can be also classified depending on the type of conceptual setting considered to derive the constitutive equations. On the one hand, within classical hypoelastic framework which does not have a thermodynamic law, e.g. (Aifantis, 1984; Muhlhaus and Aifantis, 1991; Zbib and Aifantis, 1992; Fleck and Hutchinson, 1993; Zbib, 1994). Related to this type of material formulation Sluys et al. (1993) and Pamin (1994) have proposed numerical algorithms for the stress integrations at the local and finite element level. On the other hand, within a thermodynamic framework, e.g. (Dillon and Kratochvil, 1970; Acharya and Bassani, 1995), who considered strain gradient plasticity formulation which retain the essential structure of conventional plasticity and obey thermodynamic restrictions, Svedberg and Runesson (1998), who developed gradient-dependent plasticity constitutive equations whereby the non-local character is restricted to the internal variables, leading to an additive expression of the free energy density and and more recently, Voyiadjis et al. (2004), who presented a feasible thermodynamic approach to derive coupled gradient viscoplasticity and viscodamage theories.

In this work, the thermodynamically consistent gradient-dependent plasticity theory by Svedberg and Runesson (1998) is used to formulate a parabolic Drucker–Prager model for cohesive-frictional materials that includes an isotropic hardening/softening law. The particular case of small strains is considered in the analyses. The attention is also focused on the analysis of the localization properties of the non-local material model. To this end, the gradient-dependent elastoplastic localization properties are cast in the form of an elliptical envelope condition in the $\sigma_N - \tau_N$ coordinates of Mohr, see Pijaudier-Cabot and Benallal (1993), Liebe and Willam (2001). Thereby, the tangency condition between the localization ellipse and the major principal circle defines the existence of localized failure mode and the corresponding critical directions. In this work, the geometrical localization analysis for gradient-dependent parabolic Drucker–Prager elastoplasticity is defined in terms of the characteristic length that determines the degree of non-locality of the constitutive equations.

The results of the localization analysis in the Mohr coordinates demonstrate the capability of the thermodynamically consistent gradient-dependent elastoplastic Drucker–Prager model to suppress the discontinuous bifurcations of the local or classical model formulation that occur when the hardening/softening modulus $\bar{H}$ equals the critical value for localization $\bar{H}_c$, as long as the characteristic length l remains positive. However, when $\bar{H} < \bar{H}_c$, discontinuous bifurcation may be signalized by the gradient elastoplastic model if the non-local hardening/softening modulus $\bar{H}^g$ is lower than a limit value defined in terms of $\bar{H}_c$ and l. This important results indicate that the regularization capability of the thermodynamically consistent gradient-dependent Drucker–Prager elastoplastic model does depend not only on the characteristic length l but also on the relationship between $\bar{H}^g$, $\bar{H}_c$, $\bar{H}$ and l.

2. Gradient-dependent elastoplasticity

We follow the thermodynamically consistent gradient-dependent material theory by Svedberg and Runesson (1998). After reviewing the relevant thermodynamic and

constitutive equations, the parabolic Drucker–Prager gradient elastoplastic model is presented, in which the non-local character is restricted to the internal plastic variables.

2.1. Thermodynamic consistency

Under consideration of small strain kinematics, the free energy density of a strain gradient elastoplastic continuum can be expressed in an additive form as

$$\rho\Psi(\boldsymbol{\varepsilon}^{\mathrm{e}},\kappa,\nabla\kappa)=\rho\Psi^{\mathrm{e}}(\boldsymbol{\varepsilon}^{\mathrm{e}})+\rho\Psi^{\mathrm{p,loc}}(\kappa)+\rho\Psi^{\mathrm{p,g}}(\nabla\kappa), \tag{1}$$

where ρ is the material density. The elastic free energy density is defined as $\rho\Psi^{\mathrm{e}}(\boldsymbol{\varepsilon}^{\mathrm{e}})=\frac{1}{2}\boldsymbol{\varepsilon}^{\mathrm{e}}:\boldsymbol{E}^{\mathrm{e}}:\boldsymbol{\varepsilon}^{\mathrm{e}}$, being $\boldsymbol{\varepsilon}^{\mathrm{e}}$ and $\boldsymbol{E}^{\mathrm{e}}$ the elastic strain tensor and the fourth-order elastic operator, respectively.

The local and gradient free energy density contributions due to inelastic strains $\Psi^{\mathrm{p,loc}}$ and $\Psi^{\mathrm{p,g}}$ are expressed in terms of the scalar hardening/softening variable κ. We observe in Eq. (1) that the gradient effects are only restricted to hardening/softening behavior via the inclusion of $\nabla\kappa$.

From the Coleman's relations follow the constitutive equations:

$$\boldsymbol{\sigma}=\rho\frac{\partial\Psi}{\partial\boldsymbol{\varepsilon}},\quad \boldsymbol{\sigma}=\boldsymbol{E}^{\mathrm{e}}:\boldsymbol{\varepsilon}^{\mathrm{e}}, \tag{2}$$

whereby $\boldsymbol{\sigma}$ is the stress tensor and $\boldsymbol{\varepsilon}$ the strain tensor. The dissipative stress within the continuum is defined as

$$K=K^{\mathrm{loc}}+K^{\mathrm{g}} \tag{3}$$

being

$$K^{\mathrm{loc}}=-\rho\frac{\partial\Psi^{\mathrm{p,loc}}}{\partial\kappa},\quad K^{\mathrm{g}}=\nabla\cdot\left(\rho\frac{\partial\Psi^{\mathrm{p,g}}}{\partial(\nabla\kappa)}\right) \tag{4}$$

while on the boundary $\partial\Omega$, the dissipative stress due to the gradient in Eq. (4.b) turns

$$K^{(\mathrm{g,b})}=-\boldsymbol{m}\cdot\rho\frac{\partial\Psi^{\mathrm{p,g}}}{\partial(\nabla\kappa)} \tag{5}$$

with the (outward) normal $\boldsymbol{m}$ to $\partial\Omega$.

2.2. Constitutive equations

2.2.1. General case

Considering a convex set B of plastically admissible states defined as $B=\{(\boldsymbol{\sigma},K)\,|\,\Phi(\boldsymbol{\sigma},K)\leqslant 0\}$ with the convex yield function $\Phi=\Phi(\boldsymbol{\sigma},K)$, and a dissipative potential $\Phi^{*}=\Phi^{*}(\boldsymbol{\sigma},K)$, which turns Φ in case of associated plasticity. Then, the rate equations for the inelastic strains $\dot{\boldsymbol{\varepsilon}}^{\mathrm{p}}$ and the scalar hardening/softening variable $\dot{\kappa}$, take the forms

$$\dot{\boldsymbol{\varepsilon}}^{\mathrm{p}}=\dot{\lambda}\frac{\partial\Phi^{*}}{\partial\boldsymbol{\sigma}}\quad\text{and}\quad\dot{\kappa}=\dot{\lambda}\frac{\partial\Phi^{*}}{\partial K}, \tag{6}$$

where $\dot{\lambda}$ is the rate of the plastic parameter.

From the Prandtl–Reuss additive decomposition of the total strain rate tensor into the elastic and plastic components that characterized the flow theory of plasticity and considering Eqs. (2), (4) and (6) follow the constitutive equations (in rate form):

$$\dot{\boldsymbol{\sigma}} = \dot{\boldsymbol{\sigma}}^{\mathrm{e}} - \dot{\lambda}\boldsymbol{E}^{\mathrm{e}}\frac{\partial \Phi^*}{\partial \boldsymbol{\sigma}} \quad \text{with } \dot{\boldsymbol{\sigma}}^{\mathrm{e}} = \boldsymbol{E}^{\mathrm{e}} : \dot{\boldsymbol{\varepsilon}}, \tag{7}$$

$$\dot{K}^{\mathrm{loc}} = -\dot{\lambda}H\frac{\partial \Phi^*}{\partial K} \tag{8}$$

and

$$\dot{K}^{\mathrm{g}} = l^2\nabla\cdot\boldsymbol{H}^{\mathrm{g}}\cdot\left[\nabla\dot{\lambda}\frac{\partial \Phi^*}{\partial K} + \dot{\lambda}\nabla K\frac{\partial^2 \Phi^*}{\partial K^2}\right], \tag{9}$$

which on the boundary turns

$$\dot{K}^{(\mathrm{g,b})} = -l^2\boldsymbol{m}\cdot\boldsymbol{H}^{\mathrm{g}}\cdot\left[\nabla\dot{\lambda}\frac{\partial \Phi^*}{\partial K} + \dot{\lambda}\nabla K\frac{\partial^2 \Phi^*}{\partial K^2}\right]. \tag{10}$$

In the above equations, two types of state parameters were considered. On the one hand, the *local* hardening/softening modulus H and, on the other hand, the second-order tensor of *non-local gradient* state parameters $\boldsymbol{H}^{\mathrm{g}}$ defined as

$$\boldsymbol{H}^{\mathrm{g}} = \rho\frac{1}{l^2}\frac{\partial^2 \Psi^{\mathrm{p,g}}}{\partial(\nabla\kappa)\otimes\partial(\nabla\kappa)}, \tag{11}$$

with

$$H \geqslant 0, \quad \det(\boldsymbol{H}^{\mathrm{g}}) \geqslant 0. \tag{12}$$

As pointed out by Svedberg and Runesson (1998), there are three possible interpretations for the characteristic length l in Eq. (11): as a convenient dimensional parameter which allows that both H and $\boldsymbol{H}^{\mathrm{g}}$ get the same dimension, as a physical entity that defines the characteristic measure of the microstructure and as a parameter that brings numerical stabilization to the local constitutive theory.

The Kuhn–Tucker conditions complete the rate formulation of the gradient-dependent plasticity in terms of hardening variables which, similarly to the local theory, are defined by

$$\dot{\lambda} \geqslant 0, \quad \Phi(\boldsymbol{\sigma}, K) \leqslant 0, \quad \dot{\lambda}\Phi(\boldsymbol{\sigma}, K) = 0. \tag{13}$$

Remark. In case of mixed isotropic and kinematic hardening/softening behavior, the local and gradient free energies depend on both the isotropic and the kinematic hardening/softening variables, κ and $\boldsymbol{\beta}$, respectively, i.e. $\Psi^{\mathrm{p,loc}} = \Psi^{\mathrm{p,loc}}(\kappa, \boldsymbol{\beta})$, and $\Psi^{\mathrm{p,g}} = \Psi^{\mathrm{p,g}}(\kappa, \boldsymbol{\beta})$. Therefore, Eqs. (4) turn

$$K^{\mathrm{loc}} = -\rho \frac{\partial \Psi^{\mathrm{p,loc}}}{\partial \kappa}, \quad \boldsymbol{B}^{\mathrm{loc}} = -\rho \frac{\partial \Psi^{\mathrm{p,loc}}}{\partial \boldsymbol{\beta}} \tag{14}$$

196 and

$$K^{\mathrm{g}} = \nabla \cdot \left(\rho \frac{\partial \Psi^{\mathrm{p,g}}}{\partial (\nabla \kappa)} \right), \quad \boldsymbol{B}^{\mathrm{g}} = \nabla \cdot \left(\rho \frac{\partial \Psi^{\mathrm{p,g}}}{\partial (\nabla \boldsymbol{\beta})} \right), \tag{15}$$

199 whereas $\boldsymbol{B} = \boldsymbol{B}^{\mathrm{loc}} + \boldsymbol{B}^{\mathrm{g}}$ is the *back-stress* due to kinematic hardening/softening.

200 *2.2.2. Parabolic Drucker–Prager Material*

201 The expression of the second order Drucker–Prager yield criterium yields

$$\Phi = J_2 + \mu_{\mathrm{f}} I_1 - k(f'_{\mathrm{t}} + K), \tag{16}$$

205 with J_2 the second invariant of the deviatoric stress tensor s and I_1 the first invariant
206 of the stress tensor $\boldsymbol{\sigma}$.

207 The parameters μ_{f} and k represent the material friction and cohesion, respectively.
208 When expressed in terms of the uniaxial compressive and tensile strength f'_{c} and f'_{t},
209 they take the form

$$\mu_{\mathrm{f}} = \frac{f'_{\mathrm{c}} - f'_{\mathrm{t}}}{3}, \quad k = \frac{f'_{\mathrm{c}}}{3}. \tag{17}$$

212 The explicit expression of K in Eq. (16) follows from Eqs. (3) and (4), where the local
213 and gradient free energy densities take now the forms

$$\rho \Psi^{\mathrm{p,loc}} = \tfrac{1}{2} H \kappa, \tag{18}$$

$$\rho \Psi^{\mathrm{p,g}} = \tfrac{1}{2} l^2 \nabla \kappa \cdot \boldsymbol{H}^{\mathrm{g}} \cdot \nabla \kappa. \tag{19}$$

218 Therefore, the components K^{loc} and K^{g} of K result

$$K^{\mathrm{loc}} = -H\kappa, \tag{20}$$

$$K^{\mathrm{g}} = l^2 \nabla \cdot (\boldsymbol{H}^{\mathrm{g}} \cdot \nabla \kappa). \tag{21}$$

223 To account for the volumetric dilatancy of cohesive-frictional materials in the low
224 confinement regime a pressure-sensitive plastic potential for non-associated flow is
225 considered as

$$\Phi^* = J_2 + \mu_{\mathrm{q}} I_1 - k(f'_{\mathrm{t}} + K) + g_k K^2, \tag{22}$$

228 where g_k is a constant. The flow and softening rules read then

$$\dot{\boldsymbol{\varepsilon}}^{\mathrm{p}} = \dot{\boldsymbol{s}} + \mu_{\mathrm{q}} \boldsymbol{I} \quad \text{and} \quad \dot{\kappa} = -k\dot{\lambda}, \tag{23}$$

231 with $\boldsymbol{I}$, the second-order identity tensor.

232 Associated flow is obtained when the dilatancy angle μ_{q} coincides with the friction
233 angle μ_f and $g_k = 0$.

3. Localized failure condition

From the Continuum Mechanic's viewpoint, localized failure modes are related to discontinuous bifurcations of the equilibrium path, and lead to the lost of ellipticity of the equations that govern the static equilibrium problem.

The inhomogeneous or localized deformation field exhibits a plane of discontinuity that can be identified by the singularity condition of the acoustic or localization second order tensor, see a.o. Ottosen and Runesson (1991) and Willam and Etse (1990).

The particular case of purely isotropic hardening/softening material behavior is considered in what follows as the parabolic Drucker–Prager formulation in this work is mainly used to model cohesive-frictional material behaviors which do not exhibit kinematic hardening/softening.

Local and gradient flow theories of plasticity result both in the tangential equation that reads

$$\dot{\boldsymbol{\sigma}} = \boldsymbol{E}^{\mathrm{ep}} : \dot{\boldsymbol{\varepsilon}}, \tag{24}$$

where $\boldsymbol{E}^{\mathrm{ep}}$ denotes the elastoplastic material operator that can be expressed by means of the encompassing equation

$$\boldsymbol{E}^{\mathrm{ep}} = \boldsymbol{E}^{\mathrm{e}} - \frac{1}{(h + h_{\mathrm{g}})} \boldsymbol{E}^{\mathrm{e}} : \frac{\partial \Phi^*}{\partial \boldsymbol{\sigma}} \otimes \frac{\partial \Phi}{\partial \boldsymbol{\sigma}} : \boldsymbol{E}^{\mathrm{e}}, \tag{25}$$

with the *local* and *non-local* generalized plastic moduli

$$h = \frac{\partial \Phi}{\partial \boldsymbol{\sigma}} : \boldsymbol{E}^{\mathrm{e}} : \frac{\partial \Phi^*}{\partial \boldsymbol{\sigma}} + \bar{H} \tag{26}$$

and

$$h^{\mathrm{g}} = \begin{cases} 0 & \text{for local plasticity;} \\ \boldsymbol{n}_l \cdot \bar{\boldsymbol{H}}^{\mathrm{g}} \cdot \boldsymbol{n}_l \left(\frac{2\pi l}{\delta}\right)^2 & \text{for gradient} - \text{dependent plasticity.} \end{cases} \tag{27}$$

Being $\boldsymbol{n}_l$ the normal direction to the discontinuous surfaces, and

$$\bar{H} = H \frac{\partial \Phi}{\partial K} \frac{\partial \Phi^*}{\partial K}, \tag{28}$$

$$\bar{\boldsymbol{H}}^{\mathrm{g}} = \boldsymbol{H}^{\mathrm{g}} \frac{\partial \Phi}{\partial K} \frac{\partial \Phi^*}{\partial K}. \tag{29}$$

From Eq. (29) and for the particular case of gradient isotropy, we obtain

$$\bar{\boldsymbol{H}}^{\mathrm{g}} = \bar{H}^{\mathrm{g}} \boldsymbol{I} \tag{30}$$

with $\bar{H}^{\mathrm{g}}$ a positive, nonzero scalar. As $\boldsymbol{n}_l$ is a unit vector, results

$$\boldsymbol{n}_l \cdot \bar{\boldsymbol{H}}^{\mathrm{g}} \cdot \boldsymbol{n}_l = \bar{H}^{\mathrm{g}} \tag{31}$$

and, from Eq. (27-b)

$$h^{\mathrm{g}} = \bar{H}^{\mathrm{g}} \left(\frac{2\pi l}{\delta}\right)^2. \tag{32}$$

In case of localized failure forms associated with discontinuous bifurcation, we resort to the gradient elastoplastic localization tensor defined as

$$\boldsymbol{Q}^{\mathrm{epg}} = \boldsymbol{Q}^{\mathrm{e}} - \frac{1}{h + h^{\mathrm{g}}} \boldsymbol{a}^{*} \otimes \boldsymbol{a}, \tag{33}$$

with the elastic-localization tensor

$$\boldsymbol{Q}^{\mathrm{e}} = \boldsymbol{n}_l \cdot \boldsymbol{E}^{\mathrm{e}} \cdot \boldsymbol{n}_l \tag{34}$$

and

$$\boldsymbol{a}^{*} = \frac{\partial \Phi^{*}}{\partial \boldsymbol{\sigma}} : \boldsymbol{E}^{\mathrm{e}} \cdot \boldsymbol{n}_l, \tag{35}$$

$$\boldsymbol{a} = \frac{\partial \Phi}{\partial \boldsymbol{\sigma}} : \boldsymbol{E}^{\mathrm{e}} \cdot \boldsymbol{n}_l. \tag{36}$$

The localized failure condition in case of gradient-dependent elastoplasticity

$$\det(\boldsymbol{Q}^{\mathrm{epg}}) = 0 \tag{37}$$

leads to the analysis of the spectral properties of $\boldsymbol{Q}^{\mathrm{epg}}$. Its smallest eigenvalue, with respect to the metric defines by Q^{e}, has the expression

$$\lambda^{(1)} = 1 - \frac{\boldsymbol{a}(\boldsymbol{n}_l) \cdot [\boldsymbol{Q}^{\mathrm{e}}(\boldsymbol{n}_l)]^{-1} \cdot \boldsymbol{a}^{*}(\boldsymbol{n}_l)}{h + h^{\mathrm{g}}} = 0. \tag{38}$$

In case of gradient isotropy, the explicit form of Eq. (38) turns

$$\mathscr{H} + \frac{\partial \Phi}{\partial \boldsymbol{\sigma}} : \boldsymbol{E}^{\mathrm{e}} : \frac{\partial \Phi^{*}}{\partial \boldsymbol{\sigma}} - \boldsymbol{a} \cdot [\boldsymbol{Q}^{\mathrm{e}}]^{-1} \cdot \boldsymbol{a}^{*} = 0, \tag{39}$$

with

$$\mathscr{H} = \bar{H}_{\mathrm{c}}^{\mathrm{g}} \left(\frac{2\pi l}{\delta} \right)^{2} + \bar{H}_{\mathrm{c}}. \tag{40}$$

The localization condition in Eq. (39) serves as a basis for analytical and numerical evaluations of the localization directions $\boldsymbol{n}_l$ and of the corresponding graphical maximum hardening/softening parameters $\bar{H}_{\mathrm{c}}(\boldsymbol{n}_l) = \max[\bar{H}(\boldsymbol{n}_l)]$ in case of local plasticity, and $\bar{H}_{\mathrm{c}}^{\mathrm{g}}(\boldsymbol{n}_l) = \max[\bar{H}^{\mathrm{g}}(\boldsymbol{n}_l)]$ in gradient-dependent plasticity.

4. Geometrical method for discontinuous bifurcation in gradient-dependent parabolic Drucker–Prager elastoplasticity

In this section, the geometrical method for localization analysis is derived for the thermodynamically consistent gradient-dependent elastoplastic model formulation detailed in Section 2. The approach is based on the original proposal by Benallal (1992), which was further developed by Pijaudier-Cabot and Benallal (1993) and Liebe and Willam (2001) for classical plasticity.

Eq. (39) defines an ellipse in the $\sigma-\tau$ coordinates of Mohr

$$\sigma = \boldsymbol{\sigma} \cdot \boldsymbol{n}_l \cdot \boldsymbol{\sigma}, \quad s = \boldsymbol{n}_l \cdot \boldsymbol{s} \cdot \boldsymbol{n}_l, \tag{41}$$

$$\tau = (\boldsymbol{n}_l \cdot \boldsymbol{s}) \cdot (\boldsymbol{n}_l \cdot \boldsymbol{s}) - (\boldsymbol{n}_l \cdot \boldsymbol{s} \cdot \boldsymbol{n}_l)^2 \tag{42}$$

being $\boldsymbol{n}_l$ the normal to the plane where the Mohr components are evaluated.

For the gradient-dependent non-associated parabolic Drucker–Prager model in Section 2, we obtain

$$\frac{\partial \Phi}{\partial \boldsymbol{\sigma}} = \boldsymbol{s} + \mu_{\mathrm{f}} \boldsymbol{I}, \tag{43}$$

$$\frac{\partial \Phi^*}{\partial \boldsymbol{\sigma}} = \boldsymbol{s} + \mu_{\mathrm{q}} \boldsymbol{I}. \tag{44}$$

By adopting for the elastic tensor $\boldsymbol{E}^{\mathrm{e}}$ the form

$$\boldsymbol{E}^{\mathrm{e}} = 2G\boldsymbol{I}_4 + \Lambda \boldsymbol{I} \otimes \boldsymbol{I} \tag{45}$$

the traction vectors in Eqs. (35) and (36) can then be rewritten as

$$\boldsymbol{a}^* = 2G\boldsymbol{n}_l \cdot \boldsymbol{s} + \frac{E}{1-2v} \mu_{\mathrm{q}} \boldsymbol{n}_l, \tag{46}$$

$$\boldsymbol{a} = 2G\boldsymbol{n}_l \cdot \boldsymbol{s} + \frac{E}{1-2v} \mu_{\mathrm{f}} \boldsymbol{n}_l \tag{47}$$

and from Eq. (34) we obtain

$$[\boldsymbol{Q}^{\mathrm{e}}]^{-1} = \frac{1}{G}\left[\boldsymbol{I} - \frac{1}{2(1-v)} \boldsymbol{n}_l \otimes \boldsymbol{n}_l\right]. \tag{48}$$

The critical direction $\boldsymbol{n}_l$ and the maximum hardening/softening parameters $\bar{H}_{\mathrm{c}}$ and $\bar{H}^{\mathrm{g}}$ for localization are obtained when the Mohr circle of stresses

$$(\sigma - \sigma_{\mathrm{c}})^2 + \tau^2 = R^2 \tag{49}$$

contacts the elliptical localization envelope

$$\frac{(\sigma - \sigma_0)^2}{A^2} - \frac{\tau^2}{B^2} = 1, \tag{50}$$

where the center and radius of the Mohr circle, Eq. (49), are

$$\sigma_{\mathrm{c}} = \frac{\sigma_1 + \sigma_3}{2} \tag{51}$$

and

$$R = \frac{\sigma_1 - \sigma_3}{2}, \tag{52}$$

with σ_1 and σ_3, the major and minor principal stresses, respectively, and the center σ_0 and half axes A and B of the localization ellipse, Eq. (50), are defined by

$$\sigma_0 = \frac{1}{3} I_1 - \frac{1+v}{2(1-2v)} (\mu_{\mathrm{f}} + \mu_{\mathrm{q}}), \tag{53}$$

$$B^2 = \frac{\mathscr{H}}{4G} + J_2 + \frac{1(1+v)^2(\mu_f+\mu_q)^2}{8(1-2v)(1-v)} + \frac{1+v}{1-v}\mu_f\mu_q, \tag{54}$$

$$A^2 = 2\frac{1-v}{1-2v}B^2. \tag{55}$$

In the particular case of classical elastoplasticity, the inhomogeneous differential equation (39) turns

$$\bar{H}_c(\boldsymbol{n}_l) = -\frac{\partial \Phi}{\partial \boldsymbol{\sigma}} : \boldsymbol{E}^e : \frac{\partial \Phi^*}{\partial \boldsymbol{\sigma}} + \boldsymbol{a} \cdot [\boldsymbol{Q}^e]^{-1} \cdot \boldsymbol{a}^* \tag{56}$$

therefore, the parameter B^2 representing the vertical axis of the ellipse in Eq. (50) takes now the form

$$B^2 = \frac{\bar{H}_c}{4G} + J_2 + \frac{1(1+v)^2(\mu_f+\mu_q)^2}{8(1-2v)(1-v)} + \frac{1+v}{1-v}\mu_f\mu_q, \tag{57}$$

which agrees with the expression given by Liebe and Willam (2001) for the geometrical localization analysis of classical, parabolic Drucker–Prager elastoplasticity.

So, the thermodynamically consistent gradient-dependent plasticity formulation allows a simple extension of the geometrical localization method as demonstrated in this section. Thereby, the non-local effects in terms of the characteristic length and of the gradient hardening/softening modulus only affect the expression of the localization ellipse half axes A and B. Moreover, from Eqs. (39) and (40) we conclude that the half axis B of the gradient plasticity-based localization ellipse in Eq. (54) turns to its form in case of local plasticity formulation in Eq. (57) as the ratio $l/\delta \to 0$.

5. Localization analysis of gradient-dependent parabolic Drucker–Prager elastoplasticity

The localization properties of the thermodynamically consistent gradient-dependent, generalized Drucker–Prager model are analyzed for the plane strain state, when $\sigma_z = v(\sigma_x + \sigma_y)$. Two cases are considered. On the one hand, the case $\bar{H} = \bar{H}_c$ and, on the other hand, the case $\bar{H} < \bar{H}_c$, being $\bar{H}$ the particular hardening/softening modulus of the gradient-dependent model and $\bar{H}_c$ the critical (maximum) hardening/softening modulus for localization of the local elastoplastic model.

5.1. Case $\bar{H} = \bar{H}_c$

The geometrical localization analysis of the non-local gradient material formulation is performed for the simple shear, uniaxial compression and uniaxial tensile tests and the results are shown in Figs. 1–3, respectively. These results illustrate the influence of the characteristic length l in the mode of failure. When $l > 0$, no contact is observed between the localization ellipses of the gradient-dependent plasticity model and the Mohr circle corresponding to the analyzed limit stress state. Thus, diffuse

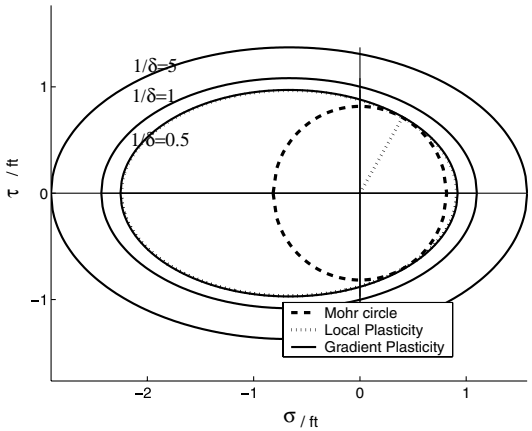

Fig. 1. Geometric localization analysis at peak of the simple shear test. Local and gradient-dependent plasticity.

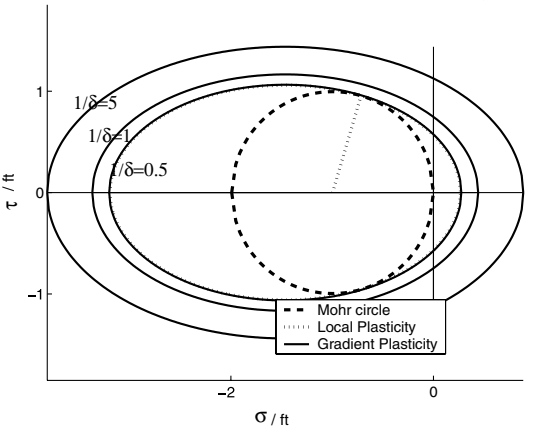

Fig. 2. Geometric localization analysis at peak of the uniaxial compression test. Local and gradient-dependent plasticity.

failure mode takes place for all three limit stress states. However, as $l/\delta \to 0$ the gradient-based localization ellipses approaches that of the local model which contacts the Mohr circle, indicating that the localization condition is fulfilled and therefore, discontinuous bifurcation takes place.

Tables 1–6, indicate the critical localization directions as well as the critical normalized hardening/softening parameter $\bar{H}_c/E$ of the classical (local) Drucker–Prager material for different strength ratios f_c'/f_t' and Poisson's modulus v. Tables 1 and 2 correspond to the limit stress state of the simple shear test, for associated and non-associated (J_2-type) plastic flows, respectively. Similarly, Tables 3 and 4 correspond to the limit stress state of the plane strain uniaxial compression test, with associated

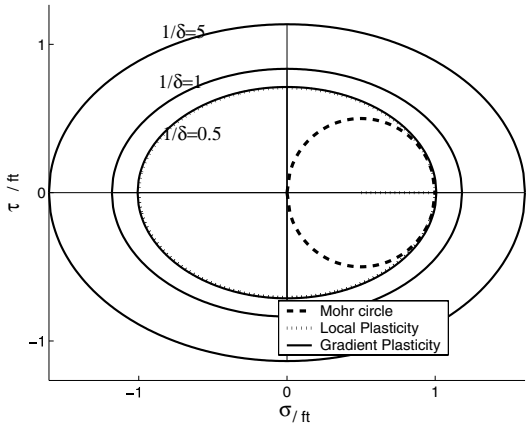

Fig. 3. Geometric localization analysis at peak of the uniaxial tensile test. Local and gradient-dependent plasticity.

Table 1
Critical localization direction θ_c and $\bar{H}_c/E$

f'_c/f'_t	$v = 0.0$		$v = 0.2$		$v = 0.4$	
	θ_c (°)	$\bar{H}_c/E$	θ_c (°)	$\bar{H}_c/E$	θ_c (°)	$\bar{H}_c/E$
2	32.9	−0.11	30.3	−0.11	27.6	−0.11
5	0.0	−1.78	0.0	−1.94	0.0	−2.23
10	0.0	−11.00	0.0	−12.30	0.0	−15.75

Simple shear test: $\mu_q = \mu_f$.

Table 2
Critical localization direction θ_c and $\bar{H}_c/E$

f'_c/f'_t	$v = 0.0$		$v = 0.2$		$v = 0.4$	
	θ_c (°)	$\bar{H}_c/E$	θ_c (°)	$\bar{H}_c/E$	θ_c (°)	$\bar{H}_c/E$
2	39.1	0.027	37.9	0.04	36.7°	0.065
5	29.4	0.44	25.8	0.667	0.0	0.88
10	0.0	2.25	0.0	3.37	0.0	4.5

Simple shear test: $\mu_q = 0$.

Table 3
Critical localization direction θ_c and $\bar{H}_c/E$

f'_c/f'_t	$v = 0.0$		$v = 0.2$		$v = 0.4$	
	θ_c (°)	$\bar{H}_c/E$	θ_c (°)	$\bar{H}_c/E$	θ_c (°)	$\bar{H}_c/E$
2	45.0	−1	36.8	−0.53	30.7	−0.21
5	39.2	−9.0	30.1	−5.63	21.9	−2.79
10	37.2	−40.11	28.0	−26.23	18.9	−13.68

Uniaxial compression test: $\mu_q = \mu_f$.

Table 4
Critical localization direction θ_c and $\bar{H}_c/E$

f'_c/f'_t	$v = 0.0$		$v = 0.2$		$v = 0.4$	
	θ_c (°)	$\bar{H}_c/E$	θ_c (°)	$\bar{H}_c/E$	θ_c (°)	$\bar{H}_c/E$
2	49.8	−0.63	42.6	−0.25	38.3	0.006
5	46.9	−4.55	39.6	−1.8	34.6	0.47
10	45.9	−18.9	38.6	−7.49	33.6	2.66

Uniaxial compression test: $\mu_q = 0$.

Table 5
Critical localization direction θ_c and $\bar{H}_c/E$

f'_c/f'_t	$v = 0.0$		$v = 0.2$		$v = 0.4$	
	θ_c (°)	$\bar{H}_c/E$	θ_c (°)	$\bar{H}_c/E$	θ_c (°)	$\bar{H}_c/E$
2	0.0	0.0	0.0	−0.03	0.0	−0.09
5	0.0	−2.0	0.0	−2.92	0.0	−4.3
10	0.0	−14.26	0.0	−25.32	0.0	−19.56

Uniaxial tensile test. $\mu_q = \mu_f$.

Table 6
Critical localization direction θ_c and $\bar{H}_c/E$

f'_c/f'_t	$v = 0.0$		$v = 0.2$		$v = 0.4$	
	θ_c (°)	$\bar{H}_c/E$	θ_c (°)	$\bar{H}_c/E$	θ_c (°)	$\bar{H}_c/E$
2	24.1	0.027	27.9	0.069	27.0	0.08
5	0.0	0.66	0.0	0.67	0.0	0.73
10	0.0	1.73	0.0	1.73	0.0	1.78

Uniaxial tensile test: $\mu_q = 0$.

409 and non-associated flows, respectively. Finally, Tables 5 and 6 are related to the
410 plane strain uniaxial tensile test. Positive values of the critical normalized harden-
411 ing/softening parameter of the local Drucker–Prager model in Tables 1–6 indicate
412 that localized failure mode in form of discontinuous bifurcation takes place before
413 peak. The results in Tables 1 and 2 agree with the well known localization properties
414 of the classical Drucker–Prager elastoplastic material in the sense that, in hardening
415 regime of the simple shear test, localized failure forms occurs for all possible Pois-
416 son's modulus and strength ratios, provide the non-associated flow rule ($\mu_q = 0$) is
417 considered. In the uniaxial compression test, a localized failure form in the pre-peak
418 regime of classical Drucker–Prager material occurs only when $v \geqslant 0.4$ in the non-
419 associated flow rule ($\mu_q = 0$), as can be observed in Table 4. Finally, in the uniaxial
420 tensile test localized failure mode takes place in the hardening regime, in both asso-
421 ciated flow rule (when $f'_c/f'_t = 2$ and $v = 0$) and non-associated flow rule (for all pos-
422 sible Poisson's moduli and strength ratios).
423 The results in Figs. 1–3 demonstrate that the non-local gradient formulation leads
424 to the same critical directions for localization as those corresponding to the local

425 model. However, the lack of contact between the Mohr circles and the localization
426 ellipses of the gradient model, indicates that this non-local theory suppress the dis-
427 continuous bifurcation condition of the local one, for all possible ratios $l/\delta > 0$.

428 *5.2. Case:* $\bar{H} < \bar{H}_c$

429 We consider the particular case when the adopted hardening/softening modulus is
430 smaller than the critical one for localization of the local elastoplastic model formu-
431 lation, $\bar{H} < \bar{H}_c$. From Eqs. (39) and (56) we obtain

$$\bar{H}_c - \bar{H} = \boldsymbol{n}_l \cdot \bar{\boldsymbol{H}}_c^g \cdot \boldsymbol{n}_l \left(\frac{2\pi l}{\delta}\right)^2. \tag{58}$$

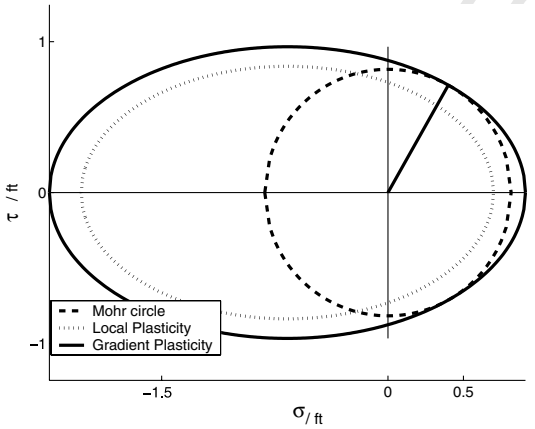

Fig. 4. Gradient localization ellipse for simple shear test and associated plasticity flow.

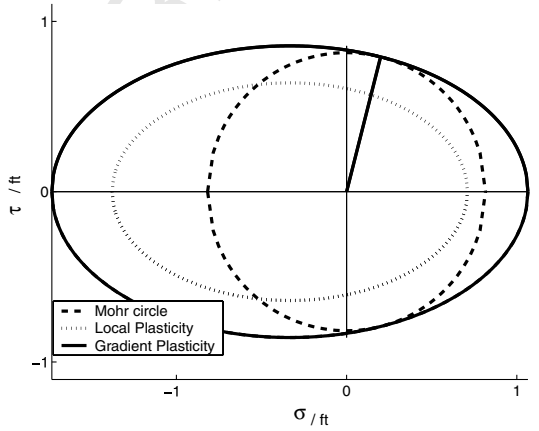

Fig. 5. Gradient localization ellipse for simple shear test and non-associated plasticity flow.

434 Therefore, the ratio δ/l results, see Svedberg (1999),

$$\frac{\delta}{l} = 2\pi\sqrt{\frac{\boldsymbol{n}_l \cdot \bar{\boldsymbol{H}}_c^g \cdot \boldsymbol{n}_l}{(\bar{H}_c - \bar{H})}}. \tag{59}$$

437 For isotropic gradient, and taking into account Eq. (31), the previous equation gives

$$\frac{\delta}{l} = 2\pi\sqrt{\frac{\bar{H}_c^g}{(\bar{H}_c - \bar{H})}}. \tag{60}$$

440 And the localization condition is then satisfied when

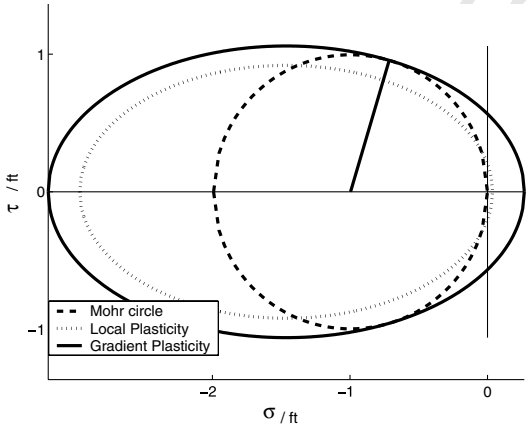

Fig. 6. Gradient localization ellipse for uniaxial compression test and associated plasticity flow.

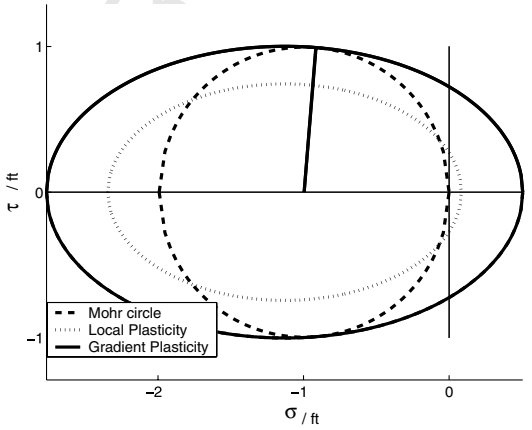

Fig. 7. Gradient localization ellipse for uniaxial compression test and non-associated plasticity flow.

$$\bar{H}_c^g = (\bar{H}_c - \bar{H})\left(\frac{\delta}{2\pi l}\right)^2. \tag{61}$$

We conclude that, when the condition in Eq. (61) is fulfilled, the gradient-dependent elastoplastic material formulation leads to localized failure modes, similarly to the local material model.

Figs. 4 and 5 exhibit the localization angles of the gradient-dependent elastoplastic model for the limit state of the simple shear test with associated and non-associated plastic flows, respectively.

The gradient localization ellipses corresponding to the limit stress state of the uniaxial compression test are presented in Figs. 6 and 7, while in Figs. 8 and 9 those corresponding to the stress state of the uniaxial tensile test.

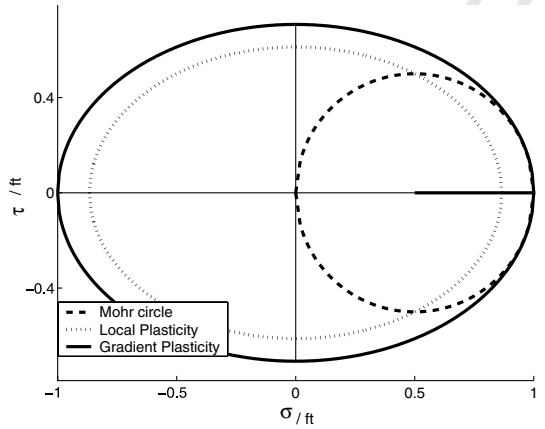

Fig. 8. Gradient localization ellipse for uniaxial tensile test and associated plasticity flow.

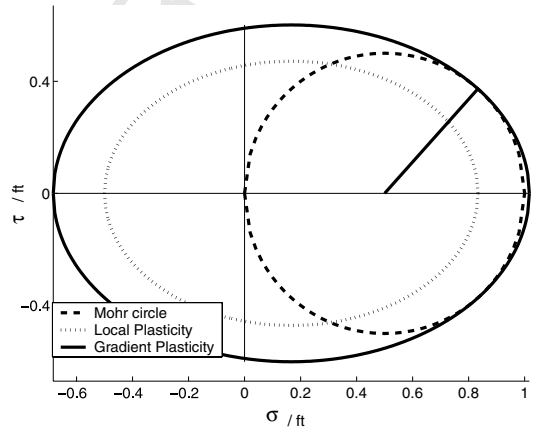

Fig. 9. Gradient localization ellipse for uniaxial tensile test and non-associated plasticity flow.

453 To verify the previous geometrical results regarding the shortcomings of the gra-
454 dient-dependent elastoplastic formulation of the parabolic Drucker–Prager model to
455 suppress discontinuous bifurcations when Eq. (61) is fulfilled, a numerical localiza-
456 tion study is performed at the constitutive level. The diagrams in Fig. 10 show the
457 variation of the normalized localization indicator $\det \boldsymbol{Q}^{epg} / \det \boldsymbol{Q}^{e}$ with the in-plane
458 failure angles for pure shear test at peak, when $\bar{H}/E = 0.5\bar{H}_c/E = 0.032$. The cases
459 corresponding to associated and non-associated gradient elastoplasticity as well as
460 non-associated local elastoplasticity were considered. The results in Fig. 10

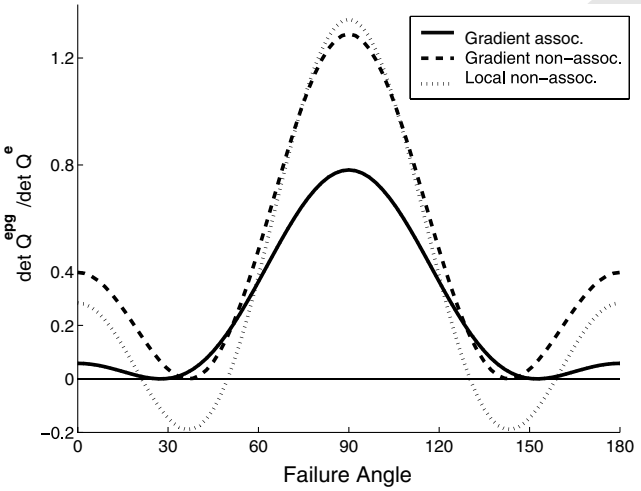

Fig. 10. Bifurcation analysis for parabolic Drucker–Prager model with $f'_c/f'_t = 2$, $\nu = 0.4$.

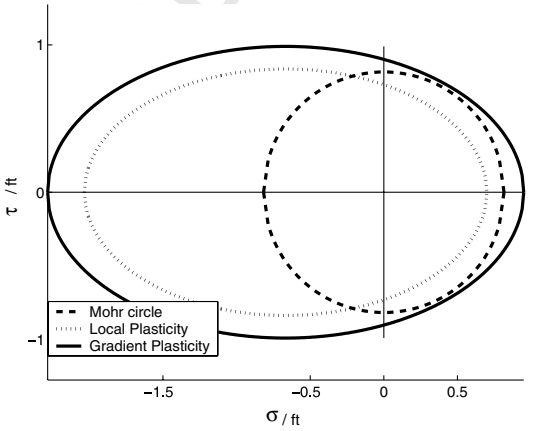

Fig. 11. Gradient localization ellipse for simple shear test at peak when $\bar{H}^g > (\bar{H}_c - \bar{H})(\delta/2\pi l)^2$. Associated plasticity.

461 demonstrate the shortcomings of the gradient-dependent elastoplastic model formu-
462 lation to eliminate discontinuous bifurcation in the form of localized failure when
463 $\bar{H} < \bar{H}_c$. In the particular case of simple shear test, the non-associated gradient-
464 dependent model leads also to localized failure in the pre-peak regime, similarly to
465 the local elastoplastic formulation.

466 By adopting a gradient modulus $\bar{H}_g$ that satisfies

$$\bar{H}^g > \bar{H}_c^g \tag{62}$$

469 the discontinuous bifurcations is suppressed. To analytically verify this, the value
470 $\bar{H}^g = 1.2(\bar{H}_c - \bar{H})(\delta/2\pi l)^2$ is assumed. The failure predictions of the resulting

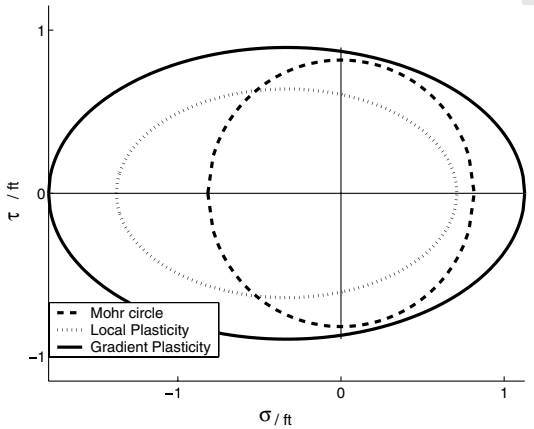

Fig. 12. Gradient localization ellipse for simple shear test at peak when $\bar{H}^g > (\bar{H}_c - \bar{H})(\delta/2\pi l)^2$. Non-associated plasticity.

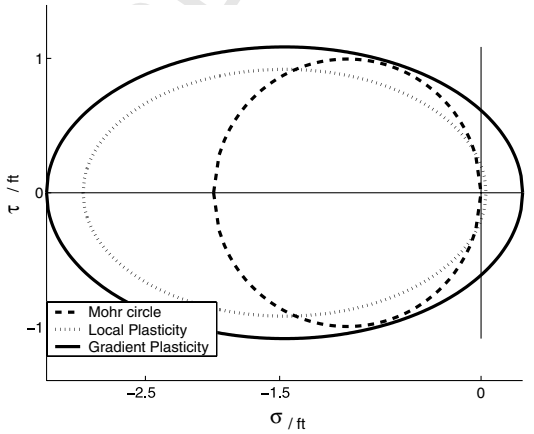

Fig. 13. Gradient localization ellipse for uniaxial compression test at peak when $\bar{H}^g > (\bar{H}_c - \bar{H})(\delta/2\pi l)^2$. Associated plasticity.

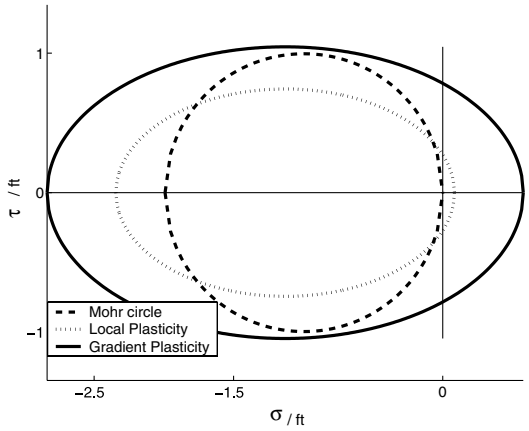

Fig. 14. Gradient localization ellipse for uniaxial compression test at peak when $\bar{H}^g > (\bar{H}_c - \bar{H})(\delta/2\pi l)^2$. Non-associated plasticity.

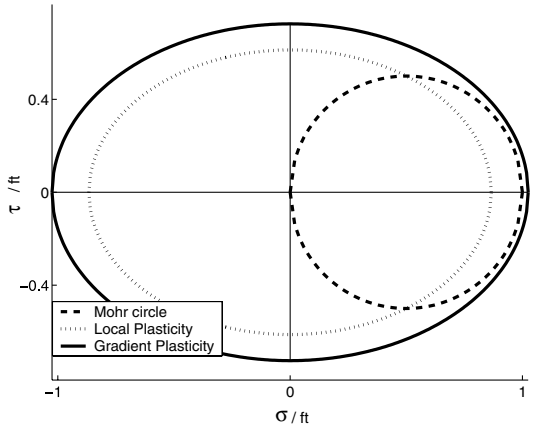

Fig. 15. Gradient localization ellipse for uniaxial tensile test at peak when $\bar{H}^g > (\bar{H}_c - \bar{H})(\delta/2\pi l)^2$. Associated plasticity.

non-local generalized Drucker–Prager elastoplastic model in terms of the localization ellipse are depicted in Figs. 11–16 for the peak stress states of the plane strain simple shear, uniaxial compression and uniaxial tensile tests. We observe the lack of contact between the localization ellipse and the Mohr circle, indicating that no localized failure mode takes place.

Remark. According to the classification of strain gradient plasticity theories by Huang et al. (2004), the constitutive theory considered in this work belongs to the so-called lower-order theory as it does not involve higher order stresses and the plastic strain gradients appear only at the constitutive level, while the boundary conditions

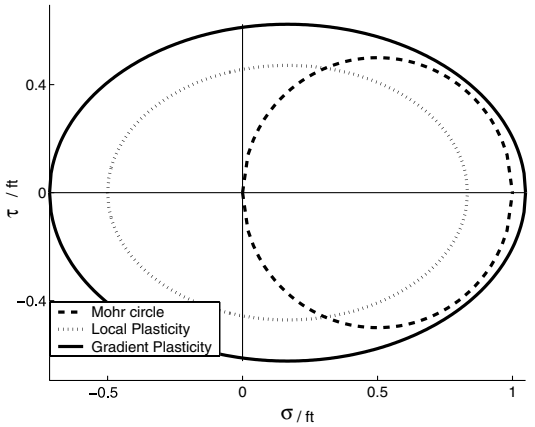

Fig. 16. Gradient localization ellipse for uniaxial tensile test at peak when $\bar{H}^{g} > (\bar{H}_c - \bar{H})(\delta/2\pi l)^2$. Non-associated plasticity.

are the same as in the classical or local plasticity. Actually, as shown in the same work by Huang et al. (2004), both lower and higher order strain gradient theories lead to similar stress distributions away from a thin boundary layer of the solid. However, as the localization bands may represent internal boundaries in the continuum it is expected that the localization solutions corresponding to the two different gradient plasticity theories, obtained with geometrical and/or analytical methods, would differ.

6. Conclusion

In this work, a geometrical localization method was developed for the analysis of the discontinuous bifurcation properties of the thermodynamically consistent gradient-dependent parabolic Drucker–Prager elastoplastic model for cohesive-frictional materials. The gradient-dependent elastoplastic localization condition was expressed in terms of the coordinates of Mohr to obtain a second-order ellipse that represents the envelope of localization for each particular state of stress. The localization condition was geometrically defined by the tangency condition between the localization ellipse and the major principle circle of Mohr, while the mode of failure was defined by the inclination of the Mohr circle radio to the tangential point with the localization ellipse.

The results of the geometrical localization analysis indicate that the gradient-dependent parabolic Drucker–Prager elastoplastic formulation suppresses the discontinuous bifurcations of the classical elastoplasticity when the selected hardening/softening modulus $\bar{H}$ equals the critical one for localization of the local material formulation $\bar{H}_c$.

The regularization capability of the gradient formulation reduces as $l/\delta \to 0$. Therefore, the characteristic length l defines the level of diffusion of the failure

mode. When l approaches zero, a continuous transition from non-local gradient to local elastoplasticity is obtained. In the extreme case, when $l = 0$, see Eqs. (40), (54) and (57), the local formulation is fully recovered. On the other hand, by adopting a hardening/softening modulus $\bar{H} < \bar{H}_c$, the gradient elastoplastic material formulation may lead to localized failure modes, as long as the non-local gradient hardening/softening modulus $\bar{H}^g$ is lower than a limit value defined in terms of $\bar{H}_c$ and l. Therefor, we conclude that regularization capability of the thermodynamically consistent gradient-dependent plasticity formulation does not only depends on the characteristic length l but also on the relationship between $\bar{H}^g$, $\bar{H}_c$, $\bar{H}$ and l.

Acknowledgments

The authors acknowledge the financial support for this work by FONCYT (Argentina Agency for the promotion of research and technology) through the Grant No. PICT 12/9870. The second author acknowledge the partial financial support to this work by CONICET (National Council for science and technology) through Grant No. PIP 3006 and by the University of Tucuman, Argentina, through the Grant No. 26/E217.

References

Acharya, A., Bassani, J.L., 1995. On non-local flow theories that preserve the classical structure of incremental boundary value problems. In: Pineau, A., Zaoul, A. (Eds.), IUTAM Sumposium of Micromechanics of Plasticity and Damage of Mulitphase Materials. Kluwer Academic Publishers, Dodretch, pp. 3–9.

Aifantis, EC, 1984. On the microstructural origin of certain inelastic models. Trans. ASME J. Eng. Mater. Technol. 106, 326–330.

Bažant, Z.P., 1986. Mechanics of distributed cracking. Appl. Mech. Rev. 3, 675–705.

Benallal, A., 1992. On localization phenomena in thermo-elasto-plasticity. Arch. Mech. 44, 15–29.

Dillon, O., Kratochvil, J., 1970. A strain gradient theory of plasticity. Int. J. Solids Struct. 6, 1513–1533.

Etse, G., Willam, K., 1999. Failure analysis of elasto-viscoplastic material models. ASCE, J. Eng. Mech. 125, 60–69.

Fleck, N.A., Hutchinson, J.W., 1993. A phenomenological theory for strain gradient effects in plasticity. J. Mech. Phys. Solids 41, 1825–1857.

Gao, H., Huang, Y., Nix, W.D., Hutchinson, J.W., 1999. Mechanism-based strain gradient plasticity – i. Theory. J. Mech. Phys. Solids 47, 1239–1263.

Hill, R., 1962. Acceleration waves in solids. J. Mech. Phys. Solids 10, 1–16.

Huang, Y., Qu, S., Hwang, K.C., Li, M., Gao, H., 2004. A conventional theory of mechanism-based straingradient plasticity. Int. J. Plast. 20, 753–782.

Liebe, T., Willam, K., 2001. A gradient-enhaced damage for quasi-brittle materials. Int. J. Numer. Mech. 39, 3391–3403.

Muhlhaus, H.B., Aifantis, E.C., 1991. A variational principle for gradient plasticity. Int. J. Solids 28, 845–857.

Nadai, A., 1931. Plasticity. McGraw-Hill, New York.

Ottosen, N.S., Runesson, K., 1991. Properties of discontinuous bifurcation in elasto-plasticity. Int. J. Solids Struct. 27, 401–421.

Pamin, J. 1994. Gradient-dependent plasticity in numerical simulation of localization phenomena. Ph.D. thesis, TU-Delft, The Netherlands.

Perič, D., 1990. Localized deformation and failure analysis of pressure sensitive granular materials. Ph.D. thesis, University of Colorado, CEAE Dept., Boulder, USA.

Pijaudier-Cabot, G., Benallal, A., 1993. Strain localization and bifurcation in a non-local continuum. Int. J. of Solids and Structures 30, 1761–1775.

Abu Al-Rub Rashid, K., Voyiadjis, G., 2004. Analytical and experimental determination of the material intrinsic length scale of strain gradient plasticity theory from micro- and nano-indentation experiments. Int. J. Plast. 20, 1139–1182.

Rizzi, E., Carol, I., Willam, K., 1995. Conditions for the localization of deformation in pressure-sensitive dilatant materials. J. Mech. Phys. Solids 121 (4), 541–554.

Rudnicki, J., Rice, J., 1975. Localization analysis of elastic degradation with application to scalar damage. ASCE J. Eng. Mech. 23, 371–394.

Sluys, L.J., 1992. Wave propagation, localization and dispersion in softening solids. Ph.D. thesis, University of Technology, Delft, The Netherlands.

Sluys, L.J., de Borst, R., Mühlhaus, M., 1993. Wave propagation, localization and dispersion in a gradient-dependent medium. Int. J. Solids Struct. 30, 1153–1171.

Sobh, N., 1987. Bifurcation analysis of tangential material operators. Ph.D. thesis, University of Colorado, CEAE Dept., Boulder, USA.

Svedberg, T., 1999. On the modelling and numerics of gradient-regularized plasticity coupled to damage. Ph.D. thesis, Chalmers University of Technology, Sweden.

Svedberg, T., Runesson, K., 1998. A thermodynamically consistent theory of gradient-regularized plasticity coupled to damage. Lincentiate Thesis, Chalmers University of Technology, Sweden.

Thomas, T.Y., 1961. Plastic Flow and Fracture in Solids. Academic Press, London.

Voyiadjis, G., Abu Al-Rub Rashid, K., Palazotto, A.N., 2004. Thermodynamic framework for coupling of non-local viscoplasticity and non-local anisotropic viscodamage for dynamic localization problems using gradient theory. Int. J. Plast. 20, 981–1038.

Willam, K., Bicanic, N., Sture, S., 1984. Constitutive and computational aspects of strain-softening and localization in solids. In: ASME/WAM Symposium on Constitutive Equations, Macro and Computational Aspects, New OrleansASME Symposium, vol. G00274. ASME Press, New York, pp. 233–252.

Willam, K., Etse, G., 1990. Failure assement of the extended leon model for plain concrete. SCI-C.

Zbib, H.M., 1994. Size effects and shear banding in viscoplasticity with kinematic hardening. ASME, Mater. Instab. 92, 19–33.

Zbib, H.M., Aifantis, E.C., 1992. On the gradient-dependent theory of plasticity and shear banding. Acta Mech. 92, 209–225.